Influence of dissipation and effective interaction on the dense plasma dynamic structure factor

Yongjun Choi [1] and Michael S. Murillo[2]
[1]*Institute for Cyber-Enabled Research, Michigan State University, East Lansing, Michigan 48824, USA*
[2]*Computational Mathematics, Science and Engineering, Michigan State University, East Lansing, Michigan 48824, USA*

(Received 27 April 2021; accepted 1 June 2021; published 21 June 2021)

The ionic dynamic structure factor is examined to assess the relative roles of dissipation and the effective ionic interaction. Two disparate physically based models of dissipation, which can differ numerically by orders of magnitude, are used in molecular dynamics. We find a negligible impact on the amplitudes of the dynamic structure factors for physically realistic parameter values. We then examine the effective ionic interaction by varying its strength, the size of the atomic core (through a pseudopotential), and the screening model. We find that "diffusive" peaks in the dynamic structure factor are very sensitive to the form of the ionic interaction, and this sensitivity arises primarily from atomic physics through the pseudopotential. This suggests that it would be useful to employ the measured zero-frequency dynamic structure factor $S_{ii}(k, 0)$ as a constraint on the effective interaction, which in turn can be used to compute physical properties.

DOI: 10.1103/PhysRevE.103.063210

I. INTRODUCTION

The dynamic structure factor (DSF) has historically played a central role in revealing microscopic dynamics of many-body systems [1–4] because it is measured in scattering experiments and reveals density fluctuations. Advances in light sources have increased interest in the DSF. Because an experimental sample can be either deliberately preheated or heated by a probe beam, the DSF of dense plasmas is of particular interest. The basic structure of the ionic DSF of dense plasmas has been well known for decades from molecular dynamics (MD) simulations and memory function models [5]. Simple models have revealed the importance of dynamical local field corrections in determining the locations and widths of the peaks in the DSF [6].

Recently, the DSF has been revisited for warm dense matter (WDM), with a focus on the role of dissipation caused by background species [7–9]. The interest in this problem stems from the fact that while dissipation occurs naturally and strongly in plasmas such as dusty plasmas, strong dissipation appears to be observed in WDM without as clear of an explanation, which suggests that WDM is similar to suspensions [10] and granular systems [11]. Dissipation in WDM has been studied by including collisions with background species through a Langevin model. Many MD studies of WDM have employed a Yukawa interaction with Langevin dissipation [7–9]. Most of these studies yield the expected result [10,12] that stronger dissipation favors a stronger Rayleigh peak relative to the Brillouin peak; collisions with an external bath spoil the conditions for collective motion.

Here, we examine the impact of two modeling choices on the DSF. First, we reexamine the role of dissipation with a focus on its origin. We consider two physics-based models of dissipation that have quite different origins and predict very different dissipation rates. These two models are used in MD to explore the impact of dissipation on the DSF. Despite the disparate predictions of these models, we show that both predictions for dissipation are far too small to be measurable, suggesting that dissipation plays a very small role in determining the DSF in dense plasmas. Second, because our interest is in the *ion-ion* DSF, we examine the role of the effective ionic interaction in the amplitude of the "diffusive" peak, which has, to date, been largely ignored as a source of an enhanced Rayleigh peak. We find that this interaction plays a substantial role in determining the DSF; in particular, the functional form of the interaction in Fourier space is found to be connected with specific features of the DSF.

II. LANGEVIN DYNAMICS

Consider a plasma with nuclei, with coordinates $\{\boldsymbol{r}_i(t)\}$ and velocities $\{\boldsymbol{v}_i(t)\}$ and interacting through forces $\mathbf{F}_i$, surrounded by a bath of electrons that introduce a systematic drag force $-m_i\gamma\boldsymbol{v}_i$ and a stochastic force ξ. Such system-bath dynamics are often modeled with a Langevin equation of the form

$$\boldsymbol{F}_i \approx -m_i\gamma\boldsymbol{v}_i + \xi. \tag{1}$$

Here, m_i is the mass of the ith nucleus and γ is the Langevin parameter. The parameter γ is constrained by the fluctuation-dissipation theorem, which ensures that the nuclei tend toward the electron-bath temperature T_e. Physically, γ appears as the strength of a dissipative drag force on the ions due to the electrons, and an appropriate theoretical model is needed to specify γ accurately.

Recently, Stanton, Glosli, and Murillo (SGM) [13] developed a multiscale MD model in which they used the low-velocity stopping power to model electron drag, employing the model of Skupsky [14] to include partial electron

degeneracy. Their prescription leads to the estimate

$$\gamma = \frac{4Z^2e^4m_e^2 \ln \Lambda_{\rm eff}}{3\pi\hbar^3 m_i(1+e^{-\eta})}, \tag{2}$$

where $\eta = \mu/T_e$, μ is the chemical potential, Z is the charge of the ion, e is the elementary charge, $\hbar$ is the reduced Plank constant, and $\ln\Lambda_{\rm eff}$ is the effective Coulomb logarithm. The effective Coulomb logarithm, in turn, is given by [14]

$$\ln \Lambda_{\rm eff} = \int_0^\infty dk \, \frac{k^3(1+e^{-\eta})}{(e^{\lambda_T^2 k^2/(16\pi)-\eta}+1)\left(k^2+k_{TF}^2\right)^2}, \tag{3}$$

where k is the wave number, $\lambda_T = \sqrt{2\pi\hbar^2/(m_e k_B T_e)}$ is the thermal de Broglie wavelength, k_B is the Boltzmann constant, and k_{TF} is the inverse of the Thomas-Fermi screening length. A simple interpolation formula for (3) was also given in Ref. [14]:

$$\ln \Lambda_{\rm eff} \approx \tfrac{1}{2}\left[\ln\left(1+\Lambda_0^2\right)-1\right], \tag{4a}$$

$$\Lambda_0^2 = \frac{12m_e(k_BT_e)^2}{4\pi\hbar^2e^2n_e}\left(0.37+\frac{4}{9}\eta^2\right), \tag{4b}$$

where n_e is the electron number density. We found, however, that Eq. (4) yields spurious results at low densities and temperatures; this was confirmed by evaluating Eq. (3) numerically.

Through an approximation that the integrand in Eq. (3) at large k cuts off the integral at $k_c = \sqrt{16\pi/\lambda_T^2}$, which we will refer to as the modified Skupksy (MS) model, we were able to perform the integration analytically to obtain the improved form,

$$\ln \Lambda_{\rm eff} \approx \frac{1}{2}\left[(1+\Lambda^2) - \frac{\Lambda^2}{1+\Lambda^2}\right], \tag{5a}$$

$$\Lambda^2 = \frac{8m_e}{\hbar^2}\frac{\left[(\alpha^2 k_B T_e)^{\sqrt{\pi}} + E_F^{\sqrt{\pi}}\right]^{1/\sqrt{\pi}}}{k_D^2 F'_{\frac{1}{2}}(\eta)/F_{\frac{1}{2}}(\eta)}, \tag{5b}$$

$$\alpha^2 = \frac{3e}{2}F'_{\frac{1}{2}}(\eta)/F_{\frac{1}{2}}(\eta), \tag{5c}$$

where E_F is the Fermi energy, $k_D^2 = 4\pi n_e e^2/(k_BT)$ is the Debye wave vector squared, and the function $F_{\frac{1}{2}}(\eta)$ is the standard Fermi integral

$$F_{\frac{1}{2}}(\eta) = \int_0^\infty \frac{x^{1/2}dx}{e^{x-\eta}+1}, \tag{6}$$

and is related to the electron number density by

$$n_e = \frac{(2m_e k_B T_e)^{3/2}}{2\pi^2\hbar^3}F_{\frac{1}{2}}(\eta). \tag{7}$$

A comparison between these two approximations [Eqs. (4) and (5)] and the numerical integration of Eq. (3) is shown in Fig. 1. We clearly see that the Skupsky interpolation form in (4) underestimates the Coulomb logarithm around the Fermi temperature and performs worse at lower densities, where it becomes negative. Conversely, the MS model yields almost perfect results for a wide range of densities and temperatures.

Alternatively, the Langevin parameter γ can be obtained from the Rayleigh model [15], which predicts a γ value of

$$\gamma = 2\pi\frac{m_e}{m_i}\bar{Z}\left(\frac{4\pi n_i}{3}\right)^{1/3}\sqrt{\frac{k_BT_e}{m_e}}, \tag{8}$$

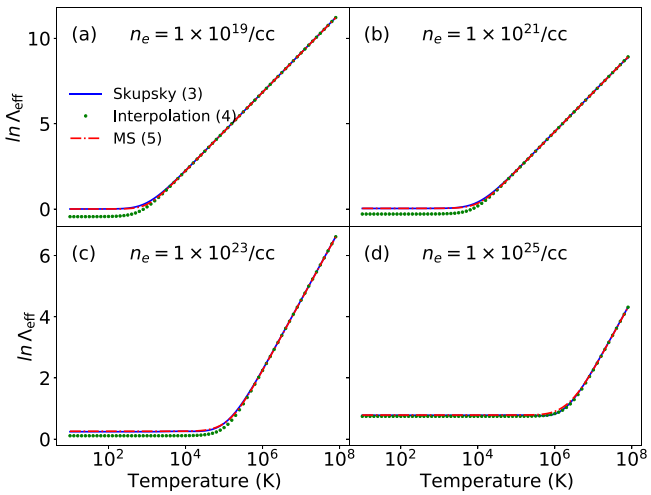

FIG. 1. Comparison of Coulomb logarithm Skupsky [Eq. (3)] with the simple interpolation of Skupsky [Eq. (4)] and with MSM [Eq. (5)] for (a) $n_e = 1\times10^{19}/cc$, (b) $n_e = 1\times10^{21}/cc$, (c) $n_e = 1\times10^{23}/cc$, and (d) $n_e = 1\times10^{25}/cc$, respectively. The simple interpolation clearly underestimates when the temperature is low, especially with a low density; moreover, in fact, the simple interpolation of the Coulomb logarithm given in [Eq. (4)] is negative in some cases [see (a) and (b)].

where n_i is the ion number density, and $\bar{Z}$ is the average ionization degree. This model is based on classical mechanics, while the SGM and MS models are based on quantum mechanics. It is worth noting the very different behaviors predicted by the SGM and Rayleigh models; for example, γ_{RM} vanishes as T_e decreases, in contrast to the SGM model, which includes Fermi degeneracy through the Skupsky stopping-power model. In addition, the dependence on $\bar{Z}$ differs between the SGM and Rayleigh models.

Figure 2 shows a comparison of the Langevin parameter among the SGM, MS, and Rayleigh models. The left panel shows the Langevin parameter for $n_i = 1.16\times10^{23}/cc$ and $Z_i = 3$. We see that the SGM model underpredicts γ by ~30% compared to the MS model when the temperature is less than

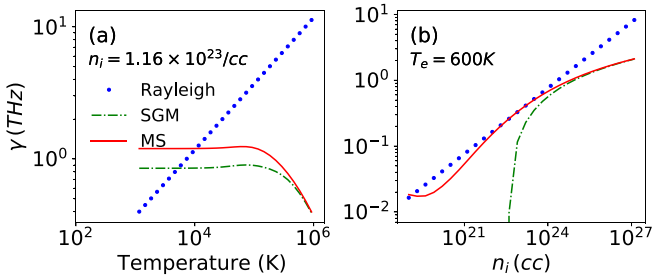

FIG. 2. Comparisons of the Langevin parameter obtained from the Rayleigh, SGM, and MS models. The left panel shows γ for $n_i = 1.16\times10^{23}/cc$ and $Z_i = 3$. The SGM model underpredicts $\gamma \sim 30\%$ compared to the MS model when the temperature is less than $\sim10^5$ K. The right panel shows γ for $T = 600$ K and $Z_i = 1$. In this case, γ predicted by the Rayleigh model is fairly close to that predicted by the MS model at low densities, but γ is overpredicted by the Rayleigh model at high densities.

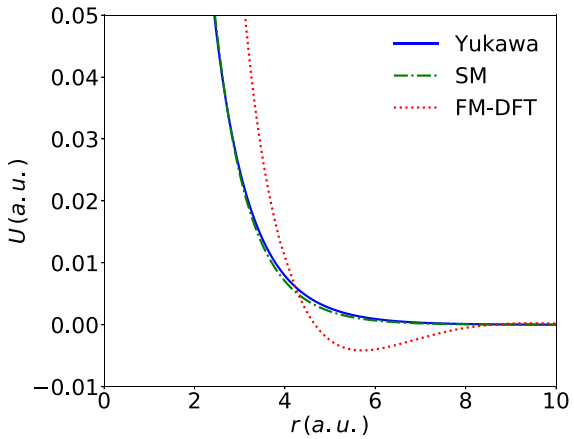

FIG. 3. A comparison of the Yukawa, SM, and force-matched density functional theory (FM-DFT) potentials for lithium, with $T = 600\,\mathrm{K}$ and $\rho = 0.513 g/cc$.

$\sim 10^5$ K. The Rayleigh model is within an order of magnitude of the MS model at low temperatures, but the difference is larger at higher temperatures. The right panel of Fig. 2 shows the Langevin parameter for $T = 600\,\mathrm{K}$ and $Z_i = 1$. In this case, γ predicted by the Rayleigh model is fairly close to that predicted by the MS model at low densities, but γ is overpredicted by the Rayleigh model at high densities. The difference between γ predicted by the SGM model and that of the MS model increases as the density decreases, as expected based on the results shown in Fig. 1.

Next, we compared the computational models and experimental data [16] for liquid lithium at $T = 600\,\mathrm{K}$. We used the Yukawa potential, the Stanton-Murillo potential (SM) [17], and the force-matched density functional theory (FM-DFT) potential [18]. Our MD simulations employed second-order velocity-Verlet integration and a linked-cell list method with a cutoff radius $r_{\mathrm{cut}} = 8$ Å because all of the potentials we examined are short range and exponentially decrease with r. For all results presented, we simulated 10^4 particles with a time step of $dt = 0.01/\omega_i$, where ω_i is the ion plasma frequency, and data were collected over $N = 80\,000$ time steps based on the convergence test by Choi *et al.* [19]. All results are averaged over 20 runs.

Figure 3 shows these three potentials for lithium, with temperature $T = 600\,\mathrm{K}$ and $\rho = 0.513/cc$ (we assume $\overline{Z} = 1$ for the Yukawa and SM potentials). The Yukawa and SM potentials are very similar and are always repulsive, whereas the FM-DFT potential has attractive regions.

Figure 4 shows the DSF from MD ($T = 600\,\mathrm{K}$ and $\rho = 0.513/cc$) and experimental data [16] for three different wave numbers. In Fig. 4, the DSFs calculated using the Yukawa, SM, and FM-DFT potentials are shown in the left, middle, and right columns, respectively; the (a), (b), and (c) rows show results for $k = 1.12$, 1.88, and 2.37 Å, respectively.

Each panel shows the results with no Langevin damping ($\gamma = 0$; solid blue line), the Rayleigh model ($\gamma = 2.6 \times 10^{-3}\omega_i$; green dot), the SGM model ($\gamma = 8.3 \times 10^{-4}\omega_i$; red dotted line), the MS model ($\gamma = 2.6 \times 10^{-3}\omega_i$; black dashed line), and experimental data (cross marks).

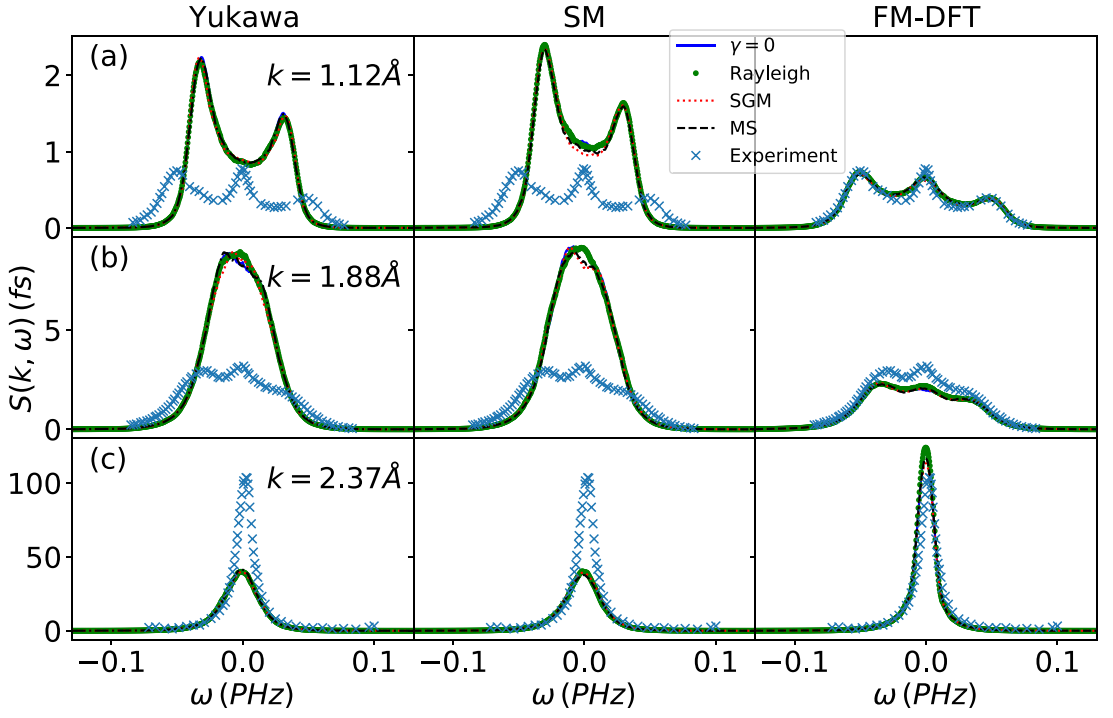

FIG. 4. Comparisons of simulation results ($T = 600\,\mathrm{K}$ and $\rho = 0.513/cc$) and experimental data [16] for three different wave numbers. The Rayleigh peak of the DSF does not depend on the Langevin parameter γ; this result is expected because γ is very small relative to ω_i. The Yukawa and SM potentials do not reproduce the experimental DSFs; however, the FM-DFT potential predicts the DSF well, revealing the sensitivity of the Rayleigh peak to the DSF.

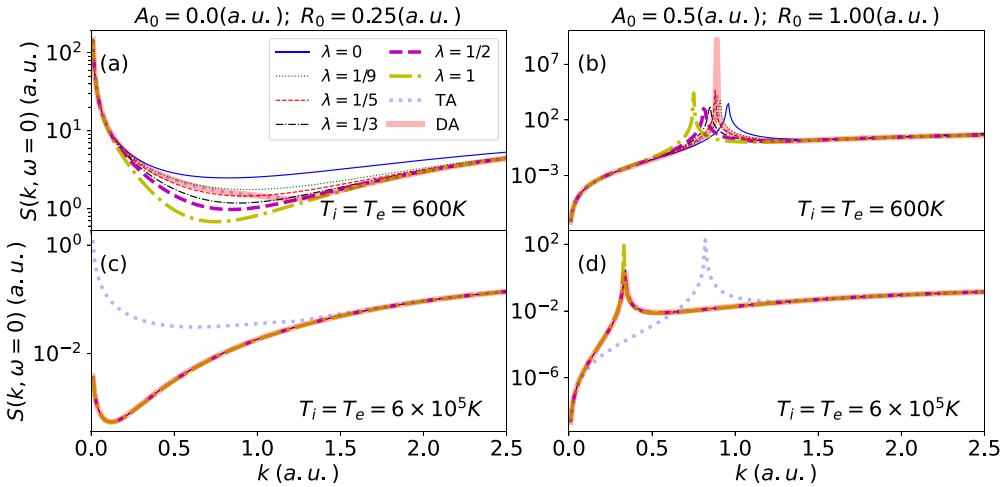

FIG. 5. The DSF $S_{ii}(k, 0)$ for various values of $\chi_{ee,0}(k)$, T_e, and $v_{ei}(k)$. (a),(b) The DSF for $T_i = T_e = 600$ K; (c),(d) the DSF for $T_i = T_e = 6 \times 10^5$ K; $\rho = 0.513/cc$. The parameter λ is a parameter in SM potentials and varies from 0 (Yukawa potential) to 1 (the traditional von Weizsäcker correction at $T_e = 0$). The amplitude of $S_{ii}(k, \omega = 0)$ is shown to depend on the $v_{ei}(k)$ at low T_e; however, this dependency decreases at higher T_e. The zero-temperature Taylor model fails to predict $S_{ii}(k, \omega = 0)$ at high temperatures, as expected.

We clearly see that neither Langevin model predicts any noticeable difference. This result is expected because γ is very small relative to ω_i, but conflicts with other reports [8,9] that have found that the DSF, especially in diffusive modes, strongly depends on γ. However, these studies employed values of γ that were 2–3 orders of magnitude larger than the values of γ examined in this study, and at such large values of γ, strong dissipation is expected.

Note that the FM-DFT model predicts the DSF well for the entire ranges of frequency and wavelength. Witte *et al.* [20] performed density functional theory molecular dynamics (DFT-MD) and reported that their simulation showed reasonable agreement with the experiment [16]. Mokshin and Galimzyanov [21] reported that a pseudopotential provided a good agreement with the experimental data [16]. This suggests the sensitivity the potential has in creating a strong Rayleigh peak in the DSF.

III. INTERACTION POTENTIALS

Given the insensitivity of the DSF to dissipation and the small electron-ion mass ratio, we can use the Born-Oppenheimer approximation to express the ionic DSF as

$$S_{ii}(k, \omega) = Im\left\{\frac{\chi_0(k, \omega)}{1 - v_{\text{eff}}(k)\chi_0(k, \omega)[1 - G_{ii}(k, \omega)]}\right\}, \quad (9)$$

$$v_{\text{eff}}(k) = \langle Z\rangle^2 v_C(k) + |v_{ei}(k)|^2 \chi_{ee}(k). \quad (10)$$

In the first line, the response-function representation, formulated in terms of the ideal-gas response $\chi_0(k, \omega)$ and the dynamic local field correction (DLFC) of ions $G_i(k, \omega)$, is used. Strong coupling (i.e., structure) is included via the DLFC, which is treated to very high accuracy in an MD implementation, whereas internal dissipation occurs in the sense of Landau damping via $\chi_0(k, \omega)$ and collisionally via the DLFC; we now focus on the remaining term: the functional form of $v_{\text{eff}}(k)$. In the second line, the effective ionic pair interaction is written in terms of the Coulomb interaction of the ionic core $v_C(k)$ and a screening term that involves the electron-ion pseudopotential $v_{ei}(k)$ and the valence-electron response function $\chi_{ee}(k)$. Writing the DSF in this representation gives insight into how the behavior of the DSF depends on the Fourier transform of the interaction; for example, if $v_{\text{eff}}(k) \approx 0$ for any k, then the measured response will be that of an ideal gas (pure Rayleigh peak), completely independent of $\chi_0(k, \omega)[1 - G_{ii}(k, \omega)]$. Similarly, the sign of $v_{\text{eff}}(k)$ determines whether a pole occurs where the denominator vanishes, $1 - v_{\text{eff}}(k)\chi_0(k, \omega)[1 - G_{ii}(k, \omega)] \approx 0$. We can understand the role of the effective interaction intuitively by neglecting the DLFC and expanding χ_0 at high frequencies to obtain $1 - v_{\text{eff}}(k)nk^2/(m\omega^2) = 0$. For the special case of pure Coulomb interactions, the dispersion relation yields a constant frequency $\omega = \omega_i$; similarly, for the Yukawa potential, an ion-acoustic dispersion $\omega = \omega_i k^2/(k^2 + k_s^2)$ is found ($k_s = 1/\lambda_s$ where λ_s is a screening length associated with properties of background). In general, however, $v_{\text{eff}}(k)$ can be oscillatory and therefore can have zero crossings and sign changes. In particular, note that for $v_{\text{eff}}(k) = 0$, the denominator is equivalent to the ideal-gas case (at that k value); there can be no peak other than $\omega = 0$.

For v_{ei}, we considered the Coulomb, Yukawa, and modified Ashcroft (MA) potentials [22]. The MA potential is

$$v_{ei}(r) = \begin{cases} A_o, & r < R_o \\ -Z/r, & r \geqslant R_o, \end{cases} \quad (11)$$

where A_o is a well depth and R_o is a radius.

For $\chi_{ee}(k)$, we considered exchange-correlation (XC) contributions at long wavelengths through the local field correction $G_{ee}(k)$ [17], given by

$$\chi_{ee}(k) = \frac{\chi_{ee,0}(k)}{1 - v_{ee}(k)\chi_{ee,0}(k)[1 - G_{ee}(k)]}, \quad (12)$$

$$G_{ee}(k) \approx \gamma_0 k^2 = \left(1 - \frac{\kappa_0}{\kappa}\right)\frac{\pi k^2}{4k_F}, \quad (13)$$

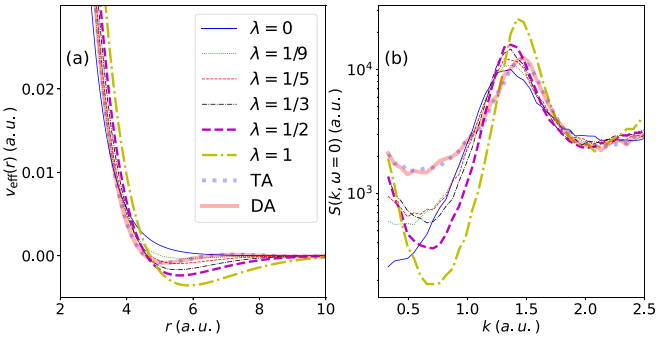

FIG. 6. Effective potentials $v_{\rm eff}(r)$ and DSF $S_{ii}(k,\omega=0)$ obtained using different approximations of $\chi_{ee,0}(k)$ (TA, DA, SMA) with $T_i = T_e = 600\,\mathrm{K}$, $\rho = 0.513/cc$. (a) $v_{\rm eff}(r)$ obtained by Fourier transformation of $v_{\rm eff}(k)$ using different approximations of $\chi_{ee,0}(k)$ (TA, DA, SMA). (b) $S_{ii}(k,\omega=0)$ obtained from MD for each potential. It can be seen that the amplitude of $S_{ii}(k,\omega=0)$ depends on $\chi_{ee,0}(k)$. Moreover, the amplitude of $S_{ii}(k,\omega=0)$ increases with λ in the SMA.

where $k_F = (3\pi^2 n_e)^{1/3}$ is the Fermi wave number, κ and κ_0 are the isothermal compressibilities for interacting and noninteracting electron gases, respectively [23], and $\chi_{ee,0}(k)$ is the usual static Lindhard response function. Detailed expressions for γ_0 can be found in Refs. [17,24,25]. For the susceptibility, we compared Taylor's zero-temperature approximation (TA) [26], Dandrea's approximation (DA) [27], and the Stanton-Murillo approximation (SMA) [17].

Figure 5 shows the DSF $S_{ii}(k,\omega=0)$ for various sets of electron temperatures, $v_{ei}(k)$ and $\chi_{ee,0}(k)$. We employ the random-phase approximation (RPA), i.e., $G_i(k,\omega)=0$, and we assume that $T_i = T_e$. The parameter λ is a factor in the SMA that varies from 0 (Yukawa potential) to 1 (the traditional von Weizsäcker correction at $T_e = 0$). Figures 5(a) and 5(c) show the DSF for $A_0 = 0.0$ and $R_0 = 0.25$, and Figs. 5(b) and 5(d) show the DSF for $A_0 = 0.5$ and $R_0 = 1.0$; Figs. 5(a) and 5(b) show the DSF for $T_i = T_e = 600\,\mathrm{K}$, and Figs. 5(c) and 5(d) show the DSF for $T_i = T_e = 6\times10^5\,\mathrm{K}$; $\rho = 0.513/cc$. The first row in Fig. 5 shows that $S_{ii}(k,\omega=0)$ depends on the the potential $v_{ei}(k)$ and on $\chi_{ee,0}(k)$ at low temperatures. However, the second row shows that $S_{ii}(k,\omega=0)$ is independent of temperature at high temperatures. The Taylor model assumes zero electron temperature and is therefore inaccurate at high temperatures. Figure 5 suggests that a strong Rayleigh peak of $S_{ii}(k,\omega)$ can arise from certain forms for the effective potential, especially adjusting $\chi_{ee,0}(k)$ at low temperatures.

In Fig. 5, we assumed the RPA for $G_{ii}(k,\omega)$. However, the RPA should not be applied when plasmas are strongly coupled. In Figs. 5(a) and 5(b), the plasma-coupling parameter Γ is 158; i.e., the plasmas being studied are strongly coupled. We performed MD simulations to determine whether a strong Rayleigh peak in $S_{ii}(k,\omega)$ can be created with a potential without using the RPA. Figure 6 shows the potentials that we examined and the corresponding $S_{ii}(k,\omega=0)$ from the MD, with $(A_0, R_0) = (0.0, 1.0)$, $\Gamma = 158$, and different values of $\chi_{ee,0}(k)$.

Figure 6(a) shows the effective potentials $v_{\rm eff}(r)$ obtained by Fourier transformation of $v_{\rm eff}(k)$ for different approximations of $\chi_{ee,0}(k)$ (TA, DA, SMA). Figure 6(b) shows $S_{ii}(k,\omega=0)$ obtained from MD simulations for each potential with $T_i = T_e = 600\,\mathrm{K}$, $\rho = 0.513/cc$. Figure 6(b) shows that the amplitude of $S_{ii}(k,\omega=0)$ depends on $\chi_{ee,0}(k)$. It also suggests that the amplitude of $S_{ii}(k,\omega=0)$ increases as λ increases in the SMA. The MD results support our argument that a strong Rayleigh peak can be obtained by adjusting $\chi_{ee,0}(k)$ in strongly coupled plasmas.

IV. CONCLUSIONS

We have examined the functional form of the plasma DSF to assess the relative contribution of dissipation and the effective ionic interaction. We considered two physically based dissipation models from very different theoretical origins to be included in our MD model. Despite the differences between these dissipation models, the Langevin parameters from these models are 2–3 orders of magnitude smaller than ω_i, and dissipation thus has a negligible impact on the DSF regardless of the ionic interaction potential employed. We also find that the FM-DFT potential predicts the functional form of the DSF reasonably well over wide ranges of frequencies and wave numbers. Next, we examined various forms of the effective ionic interaction, varying its strength, the size of the atomic core, and the form of the screening. We find that certain forms of the interaction can lead to "diffusive" peaks in the DSF and that this arises from atomic physics through the pseudopotential $v_{ei}(r)$. We also find that the sensitivity of $S_{ii}(k,\omega=0)$ to $\chi_{ee,0}(k)$ decreases with weaker coupling.

This finding suggests that the zero-frequency DSF $S_{ii}(k,\omega=0)$ can be used as a constraint on the effective interaction, which in turn can be used to compute physical properties.

ACKNOWLEDGMENTS

The authors would like to thank Luke Stanek for offering a force-matched DFT potential for lithium. This work was supported by the Air Force Office of Scientific Research under AFOSR Grant No. FA9550-17-1-0394.

[1] K. Sturm, Dynamic structure factor: An introduction, Z. Naturforsch. A **48**, 233 (1993).

[2] J. H. Chu and L. I, Direct Observation of Coulomb Crystals and Liquids in Strongly Coupled rf Dusty Plasmas, Phys. Rev. Lett. **72**, 4009 (1994).

[3] T. C. Killian, Ultracold neutral plasmas, Science **316**, 705 (2007).

[4] O. A. Hurricane, D. A. Callahan, D. T. Casey, P. M. Celliers, C. Cerjan, E. L. Dewald, T. R. Dittrich, T. Döppner, D. E. Hinkel, L. F. B. Hopkins, J. L. Kline, S. L. Pape, T. Ma, A. G. MacPhee, J. L. Milovich, A. Pak, H.-S. Park, P. K. Patel, B. A. Remington, J. D. Salmonson, P. T. Springer, and R. Tommasini, Fuel gain exceeding unity in an inertially confined fusion implosion, Nature (London) **506**, 343 (2014).

[5] J. P. Hansen and I. R. McDonald, Microscopic simulation of a strongly coupled hydrogen plasma, Phys. Rev. A **23**, 2041 (1981).
[6] S. Ichimaru, H. Iyetomi, and S. Tanaka, Statistical physics of dense plasmas: Thermodynamics, transport coefficients and dynamic correlations, Phys. Rep. **149**, 91 (1987).
[7] J. Dai, Y. Hou, J. Yuan, Unified First Principles Description from Warm Dense Matter to Ideal Ionized Gas Plasma: Electron-Ion Collisions Induced Friction, Phys. Rev. Lett. **104**, 245001 (2010).
[8] P. Mabey, S. Richardson, T. G. White, S. H. Glenzer, J. Vorberger, D. O. Gericke, A. Wierling, and G. Gregori, A strong diffusive ion mode in dense ionized matter predicted by langevin dynamics, Nat. Commun. **8**, 14125 (2017).
[9] H. Kählert, Dynamic structure factor of strongly coupled Yukawa plasmas with dissipation, Phys. Plasmas **26**, 063703 (2019).
[10] P. Pusey and R. Tough, Langevin approach to the dynamics of interacting Brownian particles, J. Phys. A: Math. General **15**, 1291 (1982).
[11] P. Maynar, M. G. de Soria, and E. Trizac, Fluctuating hydrodynamics for driven granular gases, Europhys. J. Spec. Top. **179**, 123 (2009).
[12] W. Hess and R. Klein, Generalized hydrodynamics of systems of brownian particles, Adv. Phys. **32**, 173 (1983).
[13] L. G. Stanton, J. N. Glosli, and M. S. Murillo, Multiscale Molecular Dynamics Model for Heterogeneous Charged Systems, Phys. Rev. X **8**, 021044 (2018).
[14] S. Skupsky, Energy loss of ions moving through high-density matter, Phys. Rev. A **16**, 727 (1977).
[15] A. V. Plyukhin, Generalized fokker-planck equation, brownian motion, and ergodicity, Phys. Rev. E **77**, 061136 (2008).
[16] T. Scopigno, U. Balucani, A. Cunsolo, C. Masciovecchio, G. Ruocco, and F. Sette, Inelastic X-ray scattering determination of the dynamic structure factor of liquid lithium, Philos. Mag. B **79**, 2027 (2009).
[17] L. G. Stanton and M. S. Murillo, An analytic screening potential for dense, strongly-coupled plasmas, Phys. Rev. E **91**, 033104 (2015).
[18] L. J. Stanek, R. C. ClayIII, M. W. C. Dharma-wardana, M. A. Wood, K. R. C. Beckwith, and M. S. Murillo, Efficacy of the radial pair potential approximation for molecular dynamics simulations of dense plasmas, Phys. Plasmas **28**, 032706 (2021).
[19] Y. Choi, G. Dharuman, and M. S. Murillo, High-frequency response of classical strongly coupled plasmas, Phys. Rev. E **100**, 013206 (2019).
[20] B. B. L. Witte, M. Shihab, S. H. Glenzer, and R. Redmer, Ab initio simulations of the dynamic ion structure factor of warm dense lithium, Phys. Rev. B **95**, 144105 (2017).
[21] A. V. Mokshin and B. N. Galimzyanov, Self-consistent description of local density dynamics in simple liquids. The case of molten lithium, J. Phys.: Condens. Matter **30**, 085102 (2018).
[22] M. W. C. Dharma-wardana and G. C. Aers, Determination of the pair potential and the ion-electron pseudopotential for aluminum from experimental structure-factor data for liquid aluminum, Phys. Rev. B **28**, 1701 (1983).
[23] K. Nagao, S. A. Bonev, and N. W. Ashcroft, Cusp-condition constraints and the thermodynamic properties of dense hot hydrogen, Phys. Rev. B **64**, 224111 (2001).
[24] F. Perrot and M. W. C. Dharma-wardana, Exchange and correlation potentials for electron-ion systems at finite temperatures, Phys. Rev. A **30**, 2619 (1984).
[25] M. S. Murillo, J. Weisheit, S. B. Hansen, and M. W. C. Dharma-wardana, Partial ionization in dense plasmas: Comparisons among average-atom density functional models, Phys. Rev. E **87**, 063113 (2013).
[26] R. Taylor, A simple, useful analytical form of the static electron gas dielectric function, J. Phys. F **8**, 1699 (1978).
[27] R. G. Dandrea, N. W. Ashcroft, and A. E. Carlsson, Electron liquid at any degeneracy, Phys. Rev. B **34**, 2097 (1986).